RSC Advances

PAPER

View Article Online
View Journal | View Issue



Cite this: *RSC Adv.*, 2024, **14**, 28596

# UV-driven self-replenishing liquid-infused surface with promising anti-algal adhesion performance†

Shuai Kong,[abc] Hao Wei,[d] Yan Zhang[ac] and Qingqing Rao*[e]

Received 4th June 2024
Accepted 25th August 2024

DOI: 10.1039/d4ra04077e

rsc.li/rsc-advances

Slippery liquid-infused porous surfaces (SLIPSs) inspired by *Nepenthes* have attracted much attention owing to their potential application in various cutting-edge fields. However, the performance of SLIPSs is impeded by surface damage and lubricant depletion, thereby limiting their further application. Herein, a UV-responsive slippery surface (SMEMG) was fabricated by introducing the UV-responsive functional group coumarin into the polymer side chain through random copolymerization, followed by crosslinking, curing and impregnation with vegetable oil. The self-healing ability and lubricant self-replenishing performance of the SMEMG were investigated. The results show that upon exposure to UV light, the damaged surface substrate can be repaired through a reversible photodimerization reaction between coumarin groups. Meanwhile, the lubricant oil within the bulk of the SMEMG substrate can be extruded to the surface during the photodimerization reaction, facilitating the recovery of surface wettability. The SMEMG exhibited excellent self-cleaning and anti-algal properties as well as durability in a harsh environment, demonstrating its promising application in marine anti-fouling.



## 1 Introduction

Researchers have gained a profound understanding of the biological world and have utilized biomimetics to replicate diverse functional surfaces such as anti-wetting,[1–3] self-cleaning,[4–6] and anti-fouling[7] surfaces. The study of *Nepenthes* has revealed a unique slippery surface in its prey-trapping pitcher organs, which has led to the discovery of slippery liquid-infused porous surfaces (SLIPSs).[8,9] SLIPSs have excellent liquid-repellent ability, as well as extremely low contact angle hysteresis and self-repairing capabilities.[10] Consequently, SLIPSs have demonstrated significant advantages and practical applications in marine anti-fouling,[11–13] anti-icing,[14–16] self-cleaning,[17,18] and smart liquid manipulation.[19–21]

By introducing self-healing polymers in a solid substrate, the durability of SLIPSs can be effectively improved. However, due to the inherent fluid characteristics of lubricant, they will inevitably experience loss in actual application due to external forces, such as contact, wiping, water flow impact, and the carrying of organic solvents, leading to a decline in wettability.[22] Therefore, how to timely add lubricant to the porous solid substrate, which completes the self-replenishing of SLIPSs, is crucial for enhancing their applicability. Li *et al.*[23] ingeniously utilized the structural characteristics of the earthworm skin to develop a dual-layer self-replenishing SLIPS comprising surface nanostructured membranes and square microwells that store lubricating fluid at the bottom, thereby ensuring long-lasting exceptional lubrication even in extreme conditions such as cooling, heating, and continuous droplet impact. Additionally, Zhang's group[24] introduced a novel self-replenishing SLIPS featuring primary microgrooves and secondary microcavities to address soft tissue adhesion on electrosurgical electrodes during minimally invasive surgery by storing lubricants within cavities for extended periods. Sun *et al.*[25] also reported embedding a large hole network into an inverse opal nano-porous structure as a reservoir for storing and supplying lubricants in self-replenishing applications, proposing that this achievement can be effectively applied in optical sensing, fluid transport, medical self-cleaning, and other fields. While there are several similar studies available, it should be noted that the self-healing function of these materials primarily relies on capillary forces within specially designed SLIPS structures to transport lubricants where they are needed.[26–31] However, such self-replenishing SLIPSs encounter challenges that pose difficulties in resolution through intelligent human control. The manipulation of a material's properties through light radiation has attracted considerable attention due to its ease of operation and remote controllability.[32–34] In our previous work, we fabricated an intelligent UV-responsive slippery surface using

[a]*State Grid Shandong Electric Power Research Institute, Jinan 250003, China*
[b]*College of Chemical and Biochemical Engineering, Zhejiang University, Hangzhou 310027, China*
[c]*Shandong Smart Grid Technology Innovation Center, Jinan 250002, China*
[d]*School of Life Sciences, Qufu Normal University, Qufu 273165, China*
[e]*College of Chemistry and Materials Engineering, Zhejiang A&F University, Hangzhou 311300, China. E-mail: qqrao@zafu.edu.cn*

† Electronic supplementary information (ESI) available: Figures of self-cleaning test on SMEMG by employing three typical solid particles, and the fluorescence spectra of HML, MHML, MEMG and EMG, and dynamic control of water droplet (20 μL) mobility on SEMG. See DOI: https://doi.org/10.1039/d4ra04077e

a porous substrate and silicon oil, which could achieve self-replenishment through conformational transformation of the azobenzene groups under UV light irradiation.[35]

Herein, a UV-driven self-replenishing slippery surface (SMEMG) was fabricated based on vegetable oil as the lubricant and coumarin-modified polyacrylate as the substrate. Based on the reversible photodimerization and photodepolymerization between coumarin's functional groups under UV irradiation, the polymer substrates of the SMEMG showed excellent self-healing property. Notably, photodimerization of the coumarin groups could enhance the crosslinking degree of the polymer network, resulting in the extrusion of VO within the bulk of SMEMG to its surface and thus realizing a self-replenishing of the lubricant. Furthermore, the SMEMG exhibited excellent self-cleaning and anti-algal properties as well as durability under high temperature, high-speed shear force, and a dynamic flow environment, making it a promising material for application in marine anti-fouling.

# 2 Experimental

## 2.1 Materials

4-Methylumbelliferone (HML), *tert*-butylhydroquinone (TBHQ), and *n*-hexane were obtained from Macklin. 2-Ethylhexyl acrylate (2-EHA), glycidyl methacrylate (GMA), potassium carbonate ($K_2CO_3$), *N*,*N*-dimethylacetamide (DMAc), and 2,2-azobis(2-methylpropionitrile) (AIBN) were supplied by Aladdin Chemical Reagent Co., Ltd (China). 3-Bromopropene was purchased from J&K. Acetone, ethylenediamine (ED), methyl methacrylate (MMA), butyl acetate (BuAc), dichloromethane, ethanol, and sodium chloride (NaCl) were obtained from Sinopharm Chemical Regent Co., Ltd. Vegetable oil (VO) was supplied by Arawana.

## 2.2 Fabrication of UV-responsive slippery surfaces

**2.2.1 Fabrication of 7-allyloxy-4-methylcoumarin (MHML).** HML (5.29 g), 3-bromopropene (9.68 g), and $K_2CO_3$ (13.80 g) were mixed with acetone (45.00 mL) and then stirred at 45 °C for 12 h. Afterwards, an appropriate amount of deionized water was added into the above solution to dissolve the residual $K_2CO_3$,-while dichloromethane was added to dissolve the organics. The mixed solution was then transferred into a 500 mL separating funnel for purifying. After fully shaking and becoming stratified, the mixed solution was divided into water and oil phases. The aqueous layer was removed and the organic phase was further washed with saturated salt solution at least three times. Then the crude product was gained by rotary evaporation to remove the solvents and then recrystallized with butyl acetate to obtain the refined white needle-like solid matrix, namely 7-allyloxy-4-methylcoumarin.

**2.2.2 Fabrication of P(MHML-*r*-EHA-*r*-MMA-*r*-GMA) (MEMG).** In detail, MHML (1.00 g), 2-EHA (5.00 g), MMA (3.00 g), and GMA (1.00 g) were dissolved in DMAc (6.00 g) and BuAc (9.00 g). Then the mixed solution was transferred into a 100 mL three-necked flask and fully reacted at 80 °C for 24 h, with AIBN (0.10 g) introduced as the initiator. Subsequently, the crude copolymer was refined by precipitating and dissolving with *n*-hexane and BuAc three times. Afterwards, the residual solvents were removed by drying at 60 °C to obtain the purified copolymer (MEMG). Finally, the polymer was re-dissolved in BuAc to obtain the 50 wt% polymer solution for further use. As the control, copolymer (EMG) solution was prepared in the same way without the introduction of MHML.

**2.2.3 Fabrication of the UV-responsive slippery surfaces.** In a typical experiment, the polymer solution (2.00 g) and ED (0.01 g) were uniformly blended with VO (0.25 g) by magnetic stirring for 10 min. Then the mixture was poured into the silicon mold and cured at 70 °C for 5 h to obtain the UV-responsive slippery surface (SMEMG) by using MEMG and the controlled slippery surface (SEMG) by using EMG. The substrate film was fabricated by the same method without the addition of VO, namely MEMG@ED. The slippery coatings used for the anti-adhesion test were fabricated by coating the pre-crosslinking polymer solution on blank glass and then curing at 70 °C for 5 h.

## 2.3 Characterizations

**2.3.1 Chemical structure and fluorescence property.** The chemical structures of the samples were analyzed by Fourier transform infrared (FT-IR) spectroscopy (Nicolet 5700). A SpectraMax system (M2, MD, USA) was employed to test the fluorescence intensity of the specimens. HML and MHML were dissolved in ethanol. MEMG and EMG were dissolved in butyl acetate. The excitation wavelength was 254 nm.

**2.3.2 Surface characterization.** The surface topography and surface roughness were observed by field emission scanning microscopy (SEM, Phenom prox-SED, Netherlands) and atomic force microscopy (AFM, TT2-AFM, USA) operated by multimode in the tapping mode, respectively. The scanning range was $5 \times 5$ $\mu m^2$. The surface chemical composition was evaluated by X-ray photoelectron spectroscopy (XPS, Thermo Scientific K-Alpha, USA) with an excitation source of Al K$\alpha$, $h\nu = 1486.6$ eV. The parameters for the analysis were as follows: a spot size of 400 μm, an operating voltage of 12 kV, and a filament current of 6 mA. The contact angle (CA) and droplet sliding motion were recorded on an optical contact angle goniometer (SDC-100, SINDIN Co., Ltd, China). The droplet volume for the CA tests was 2 μL and the average value was calculated by measuring at least five positions on the same sample.

**2.3.3 Stability experiments.** The durability of the SMEMG was collectively characterized by thermal stability, lubricant shear stability, flowing water stability, and vertical placement stability and evaluated by the variation of the CA on the surface of the SMEMG and the mass change of SMEMG. For the thermal stability test: The sample was placed in an oven at 80 °C and heated for 15 days. Then the CA and $\Delta m$ were measured daily to evaluate the loss of lubricant oil *via* evaporation. For testing the lubricant shear stability: The SMEMG was placed in a centrifuge (SC-3610, Anhui USTC Zonkia Scientific Instruments Co., Ltd) and rotated at 500–5000 rpm for 1 min. The sample was then taken out for further measurement. For testing the flowing water stability: The specimen was completely immersed in water with a stirring speed of 30 rpm for 80 h. The SMEMG was

taken out every few hours and then dried at 60 °C for 5 min for further analysis. For testing the vertical placement stability: the SMEMG was attached to the surface of the glass and then left upright for 15 days. The changes in the surface CA and sample mass were measured at intervals of one day to observe the gradual loss of lubricant oil.

**2.3.4 Anti-algal adhesion test.** Diatom and chlorella were employed to assess the anti-algal adhesion performance of the SMEMG. First, diatom and chlorella were incubated according to previous reports.[36] Then the specimens were immersed in the algae suspensions and then cultured at 25 °C for 24 h (12 h in light and 12 h in the dark). Afterwards, the samples were taken out, rinsed lightly with deionized water, and dried at ambient temperature. Finally, an optical microscope was used to observe the adhesion of diatom and chlorella on the surfaces of the samples.

# 3 Results and discussion

## 3.1 Fabrication and characterization of the SMEMG

As shown in Scheme 1, HML was first modified with 3-bromopropene to synthesize 7-allyloxy-4-methylcoumarin. Then the copolymer MEMG was prepared *via* a random free radical polymerization of MHML, EHA, MMA, and GMA. Subsequently, the MEMG, ED as the cross-linker, and VO as the lubricant oil were evenly mixed and then cured at 70 °C for 5 h to fabricate the UV-responsive slippery surface (SMEMG). The chemical composition of MHML, MEMG, and the substrate MEMG@ED were identified by FT-IR spectroscopy. As shown in Fig. 1a, the adsorption peak for –OH stretching vibrations was observed at 3218 $cm^{-1}$ in the FT-IR spectrum of HML, meanwhile, it had disappeared in the FT-IR spectrum of MHML. In addition, the broad brand at around 3000–2700 $cm^{-1}$ was assigned to the C–H stretching vibrations in the alkyl and aromatic ring, whereby the intensity of the C–H absorption peak on MHML was significantly higher than that on HML. Besides, signals for C=O and C=C on the coumarin ring appeared in the structure of HML at 1686 and 1609 $cm^{-1}$, and could also be found in the FT-IR spectrum of MHML slightly shifted at 1731 and 1615 $cm^{-1}$. These results demonstrated that MHML was successfully synthesized. As shown in Fig. 1b, there was an absorption peak at 1613 $cm^{-1}$ in the backbone of MEMG, suggesting that the C=C bond still existed in the structure of MEMG. However, the absorption peak intensity of C=C on MEMG was decreased compared to that on MHML. After the polymerization of MHML, 2-EHA, GMA, and MMA, most of the C=C bonds disappeared through the process of polymerization, but a small amount of C=C bonds on the coumarin ring of MHML did not participate in the polymerization. Moreover, the intensity of the C–H stretching vibration peak on MEMG at around 3000–2700 $cm^{-1}$ was further enhanced compared to that on MHML, and the characteristic absorption peak of the epoxy group was discovered at around 908 $cm^{-1}$. These results indicated that the copolymer MEMG was successfully

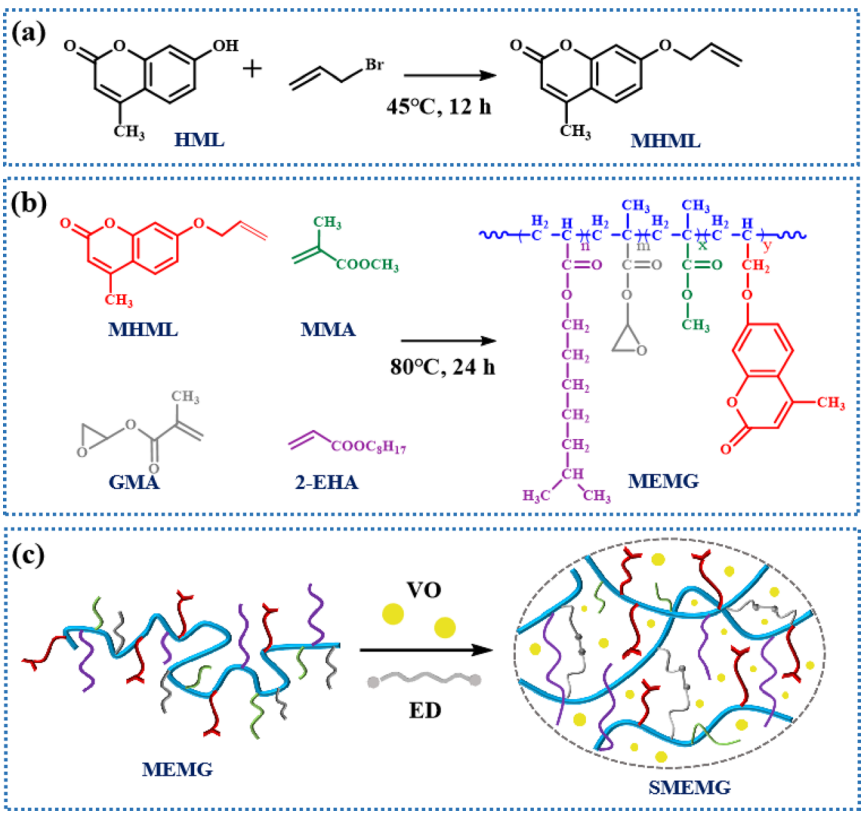


Scheme 1 Preparation procedure for the SMEMG. (a) Synthesis of 7-allyloxy-4-methylcoumarin (MHML); (b) fabrication of P(MHML-*r*-EHA-*r*-MMA-*r*-GMA) (MEMG); (c) fabrication of the UV-responsive slippery surface (SMEMG).

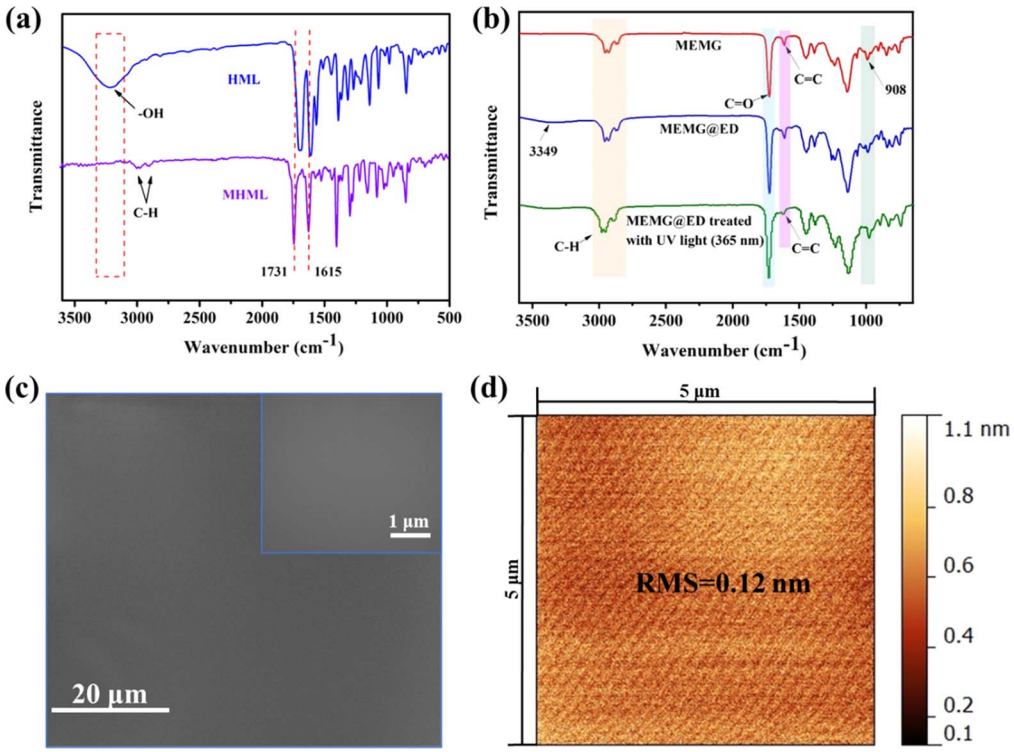


Fig. 1 (a) FT-IR spectra of HML and MHML; (b) FT-IR spectra of MEMG and MEMG@ED before and after 365 nm UV irradiation for 3 h; (c) SEM image of SMEMG; inset shows the SEM image at high magnification; (d) 2D AFM image of the SMEMG over a scope of 5 μm × 5 μm.

fabricated. Furthermore, the MEMG@ED showed a new broad band at 3349 $cm^{-1}$, which was the overlapping peak of –OH and N–H regenerated by the reaction of the epoxy group on MEMG and the amino group on ED. Besides, the absorption peak strength of the epoxy group at 908 $cm^{-1}$ was also significantly reduced after the crosslinking, indicating the successful preparation of MEMG@ED.

In this system, vegetable oil was employed as the lubricant to infuse into the substrate *via* blending and then forming the slippery surface SMEMG. Hence, the chemical affinity between the VO and MEMG@ED is crucial and could greatly affect the stability of the slippery materials. As shown in Fig. 2a, the surface of MEMG@ED exhibited an ultra-low initial VO contact angle at 0 s. Then, the VO completely spread on the surface of the substrate within 15 s, meanwhile forming a stable lubricant layer on the SMEMG. The results certified that there was a good affinity between the VO and MEMG@ED, which is conducive to the preparation of a highly stable slippery surface. Then the

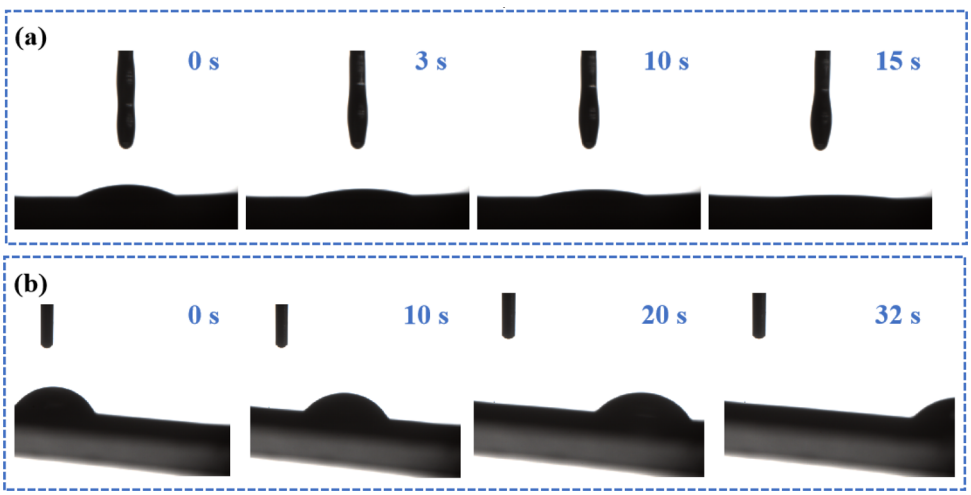


Fig. 2 (a) Photographs of VO (3 μL) spreading on the surface of MEMG@ED. (b) Photographs showing the dynamic mobility of a water droplet (7 μL) on the SMEMG with a low tilting angle (5°).

surface morphology and roughness were investigated. The SMEMG presented a defect-free smooth surface and the surface roughness was 0.12 nm, as shown in Fig. 1c and d, indicating the formation of a slippery surface with ideal smoothness. The sliding behavior of a droplet on the SMEMG was then recorded by taking digital pictures. As shown in Fig. 2b, the water droplet (7 μL) flexibly slid down the surface of the SMEMG and left no trace, suggesting the SMEMG possessed excellent slippery performance.

### 3.2 Self-healing performance

As presented in Fig. 3a, both the MEMG@ED and SMEMG exhibited good transparency, whereby the characters below could be clearly seen through the substrate film and slippery surface. After the infusion of VO into the substrate, the transparency of the SMEMG slightly declined compared to that of MEMG@ED, but it still showed favorable light transmittance owing to the good chemical affinity between the polyacrylate-based substrate and vegetable oil. Further, the lubricant oil could fill the destroyed area by capillary force and then realize the healing of the dewetting property once the SLIPS materials is damaged by external force. However, it was difficult to repair the damaged position once the skeleton substrate was broken, resulting in the loss of the slippery performance. Here, the self-healing ability of MEMG@ED was detected by cyclic "cutting–healing" tests. As shown in Fig. 3b, the broken interfaces of the substrate film were completely repaired after irradiating under UV light with a wavelength of 365 nm for 3 h and there was no obvious cutting mark on the damaged area, as shown in the optical microscopy photo. Besides, the repaired MEMG@ED presented good mechanical properties, and no tear marks appeared at the repaired fracture after tensile treatment.

To better illustrate the self-healing performance of the SMEMG, dyed and undyed samples were cut into a heart shape and then contacted with the broken interfaces without external pressure. As shown in Fig. 3c, after treatment under UV light for 3 h, the two fragments with different colors were joined in a new heart-shaped film. Similarly, the repaired SMEMG showed good mechanical strength. After stretching, the jointed SMEMG remained intact. The corresponding optical microscopy images also demonstrated the excellent self-healing ability of the SMEMG and the good mechanical property of the healed SMEMG (Fig. 3d). Besides, the dewetting properties of the SMEMG before and after healing were investigated. Here, the slippery surface was coated on the surface of an aluminum sheet. As shown in Fig. 4a, a water droplet (20 μL) easily slid down the surface of the SMEMG in 2.1 s. However, the sliding droplets would pin at the scratch after the surface was damaged by a scalpel (Fig. 4b). Nevertheless, after the scratched SMEMG was healed under UV light irradiation (Fig. 4c), the droplet re-slid down the surface (Fig. 4d), indicating the recovery of the liquid repellency ability of the SMEMG. The optical microscopy images also demonstrated the healing process of the damaged SMEMG coating (Fig. 4e, f, and h). All these results suggested that both the substrate and VO-infused slippery surface in this system have superb self-healing performance. The coumarin groups in the side chain of MEMG can undergo photo-dimerization at UV light wavelengths >300 nm, where the ethylenic group of the coumarin molecules undergo [2 + 2] cycloaddition to form a cyclobutane ring.[37–39] The evidence for

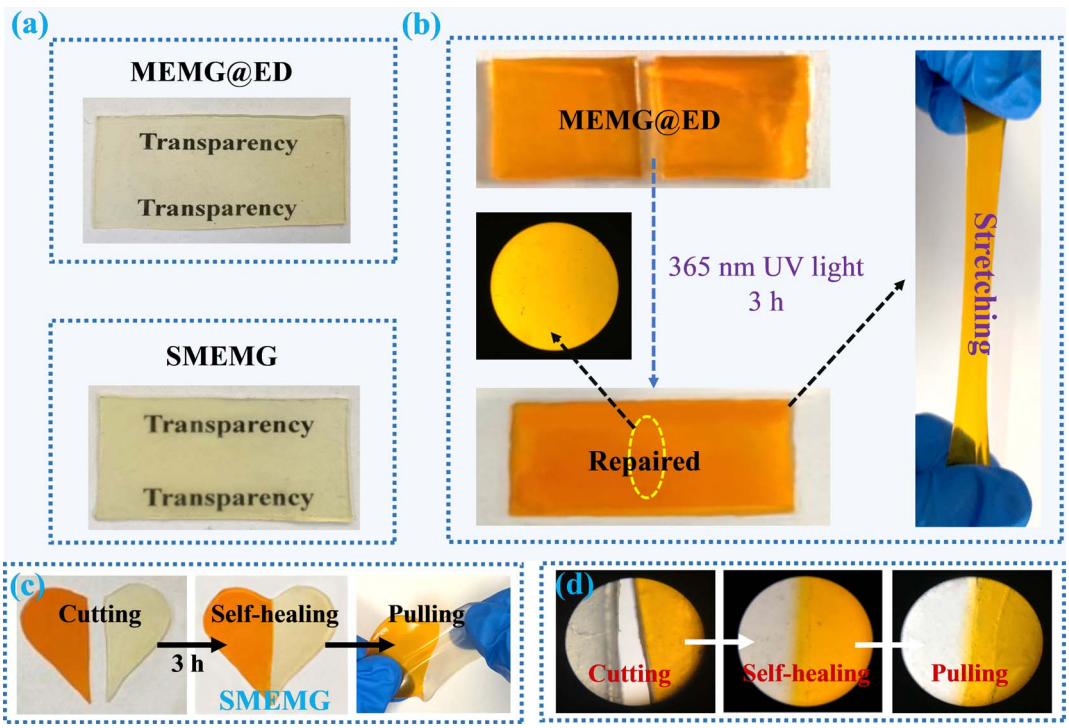


Fig. 3 (a) Digital photographs of MEMG@ED and SMEMG; (b) self-healing process of MEMG@ED; (c) self-healing process of a heart-shaped SMEMG; (d) optical microscopy images of a heart-shaped SMEMG, both MEMG@ED and the half sample of the SMEMG were dyed with Sudan I.

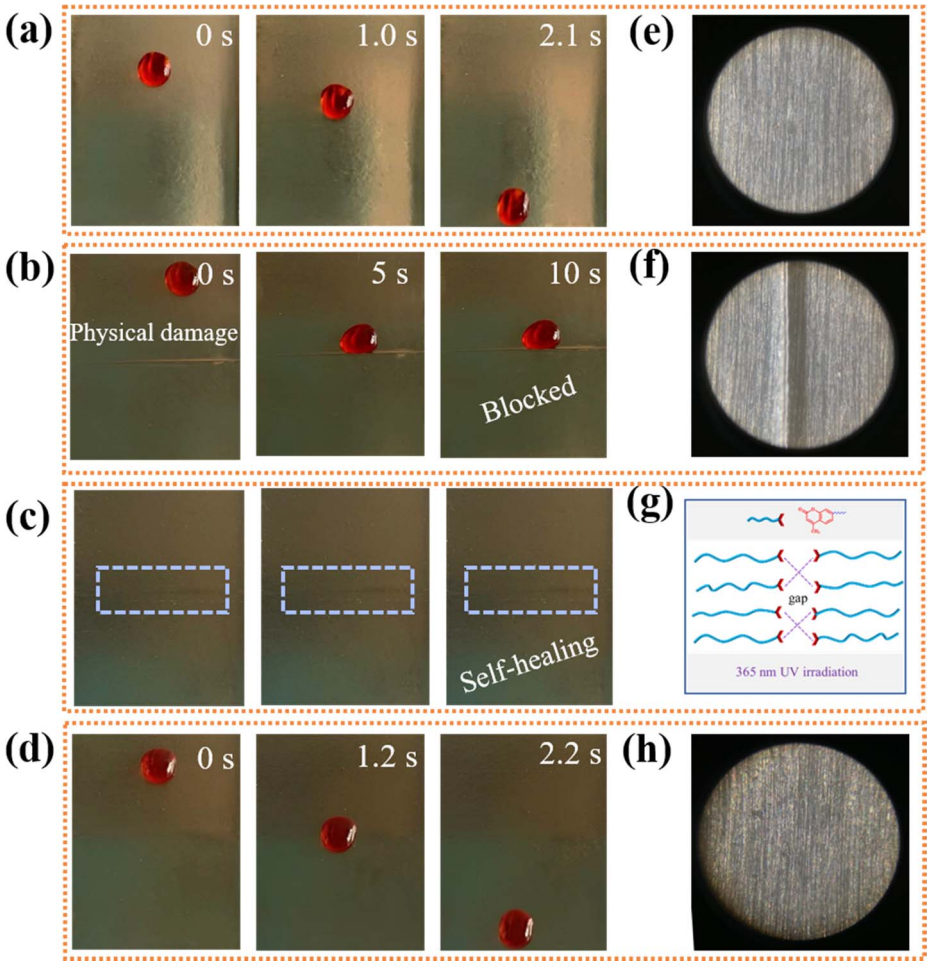


Fig. 4 Motion of a water droplet (20 μL) on the original SMEMG (a), SMEMG damaged *via* scalpel scratching, (b) and a self-healed SMEMG surface (d) under 365 nm UV light irradiation for 3 h; (c) a self-healed SMEMG surface under 365 nm UV light irradiation for 3 h. Optical microscopy images of original SMEMG (e), damaged SMEMG (f) and self-healed SMEMG surface (h). (g) Self-healing mechanism of damaged SMEMG under 365 nm UV light irradiation. The water droplet was dyed with methyl orange.

this reaction is provided in Fig. 1b, where the peak at 1613 $cm^{-1}$, corresponding to the C=C bond within the MEMG@ED spectra, exhibited a marked reduction after 3 h exposure to 365 nm UV light, confirming the occurrence of photodimerization. As a result, a new crosslinking network was formed to repair the damaged samples (Fig. 4g). Notably, the damaged matrix was preferentially irradiated under UV light at a wavelength of 254 nm for 30 min to completely photo-depolymerize the coumarin groups before healing under 365 nm UV light.

### 3.3 Self-cleaning and stability properties

In practical environments, many materials are inclined to be contaminated by complicated liquids and fine particulate matters due to their high surface energy and structural defects, thus greatly weakening the function of such materials. Here, some compound liquids in daily life were used as model pollutants to evaluate the surface self-cleaning performance of the SMEMG. As shown in Fig. 5, droplets of coffee and milk could flexibly slide down the surface of the SMEMG without any residuals. Even the sauce droplet with a complicated chemical composition and the honey droplet with ultra-high viscosity could be completely removed from the SMEMG. Whereas, these droplets were hard to slide down the surface of glass, and distinct sliding traces could be observed on the glass after liquid collecting. The defect-free surface with relatively low surface energy endowed the SMEMG with prominent anti-fouling performance. Subsequently, three typical solid particles were employed to assess the self-cleaning property of the SMEMG. As presented in Fig. S1,† a quantity of powders was firmly adhered to the surface of the SMEMG. With the water droplets sliding on the surface, the hydrophilic powders ($CuCl_2 \cdot 2H_2O$) were rapidly dissolved in the water and then carried away as the droplets slid down the surface. Differently, the hydrophobic particles ($SiO_2$ and sandy soil) floated on the liquids and then slid down with the water droplets. Benefiting from the molecular-scale smooth surface topography and good liquid repellency of SLIPS materials, these particles could not be trapped into the substrate. Therefore, the SMEMG presented a superb self-cleaning performance.

Durability is a very important factor in practical applications. However, the lubricant layer on the surface of SLIPS materials is


Fig. 5 Snapshots showing the sliding motion of coffee, sauce, milk, and honey droplets (~20 μL) on the SMEMG and glass.

really unstable due to the limited interaction between the substrate and lubricant oil. Hence, accelerated lubricant loss experiments were implemented here to detect the stability of the SMEMG. As shown in Fig. 6a, no obvious change was observed in the CA and sample mass tests after treatment at 80 °C for 15 days, indicating the SMEMG had remarkable thermal stability owing to the low volatility and high decomposition temperature of the VO. In addition, the SMEMG retained a good dewetting performance under high-speed shear force or vertical placement for 15 days (Fig. 6b and d). Moreover, the CA and mass loss of the SMEMG started to show slight increases after immersing in flowing water for 60 h. The excellent physical durability of the SMEMG was from the good compatibility between the MEMG@ED and VO. In summary, based on the synergistic effect between the excellent stability and self-healing ability of the SMEMG, the longevity of the slippery surface could

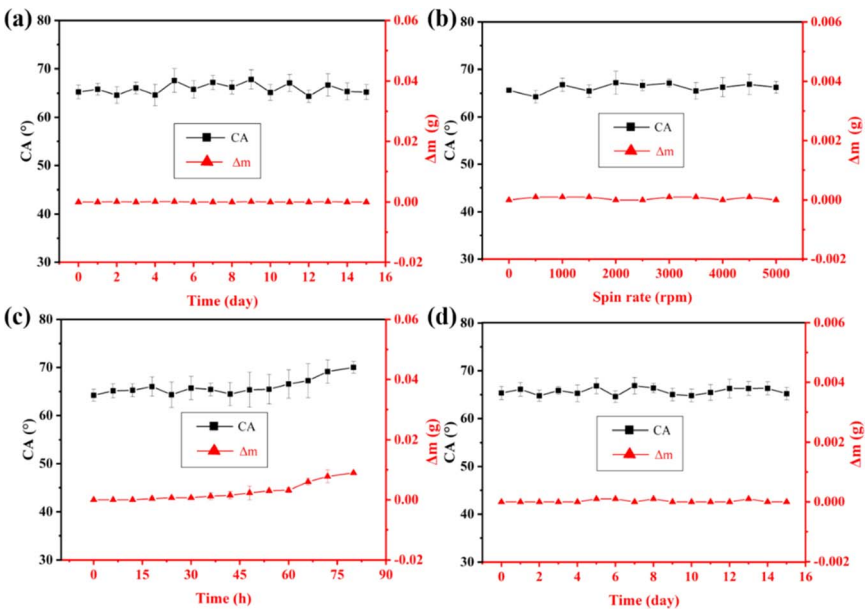


Fig. 6 Durability of the SMEMG. Variation of the CA and Δm of the SMEMG during the stability test. (a) SMEMG after heating at 80 °C for 1–15 days; (b) SMEMG rotated at 0–5000 rpm for 1 min; (c) SMEMG after immersing in water with a spin rate of 30 rpm for 80 h; (d) SMEMG placed in the vertical position for 1–15 days.

be significantly prolonged, thus promoting the practical use of the SLIPS materials.

### 3.4 Self-replenishing of the lubricant oil

Although the SMEMG exhibited prominent stability under a harsh environment, exhaustion of the surface lubricant layer for SLIPS materials is inevitable when serving in a dynamic water flow given enough time, thus resulting in the reduction of the anti-fouling performance. Interestingly, there was a strong absorption peak in the fluorescence spectra of HML, MHML, and MEMG at the wavelength range of 340–480 nm, as presented in Fig. S2.† In addition, the SMEMG showed a remarkable fluorescence phenomenon under UV light irradiation at the wavelength of 365 nm (see inset in Fig. S2c†). The results indicated that the MHML was successfully bonded into the side chain of MEMG and endowed the surface of the SMEMG with an extraordinary fluorescence effect. Based on this, we found that the SMEMG was able to respond to UV illumination at the wavelength of 365 nm, then extruding the lubricants in the bulk of substrate to the damaged surface, thus rebuilding a new lubricant layer on the surface and hence recovering the surface wettability. As shown in Fig. 7a, original SMEMG exhibited a good dewetting performance, whereby a water droplet could easily slide along the surface of the SMEMG within 2.1 s. Whereas the slippery ability of the SMEMG was immediately lost when the surface lubricant layer of the SMEMG was wiped off. As shown in Fig. 7b, the water droplet firmly stuck on the swabbed SMEMG and could not slide on the surface even after 10 s. Notably, the droplet would slide down the surface after being irradiated under UV light for 3 h in 2.2 s, thus demonstrating the re-construction of a new lubricant layer on the destroyed SMEMG. However, due to the superb chemical affinity between the vegetable oil and alkyl polyacrylate (MEMG), the oil-releasing velocity was limited. This ultra-high compatibility will promote the formation of an organogel, then restricting the extrusion of the lubricant oil. However, the low affinity will lead to the rapid loss of the lubricant.

In the initial state, the rough structure of the substrate was covered by a layer of lubricant oil, and the surface of the SMEMG was ultra-smooth with an RMS of 0.12 nm (Fig. 8a). Hence, the droplet could easily slide down the surface. After the lubricant layer was exhausted, the rough structure of the substrate became exposed at ambient environment. The roughness of the surface thus increased to 27.5 nm (Fig. 8b). The exposed rough structure would greatly enhance the hysteresis angle of a droplet, then restricting the sliding motion of the water droplet. Afterwards, based on the UV-responsive ability of coumarin groups hanging on the side chain of MEMG, the VO could be released to the damaged surface and could then reform a new liquid film on the surface. The release of the VO was corroborated by the XPS data detailed in Table S1.† The content of the C element in VO was higher than that in the substrate, while the content of the O element was lower than that in the substrate. Also, the contents of C element and O element on the surface of the SMEMG formed by the infusion of VO into the substrate were between those of the VO and the MEMG@ED. When the surface lubricant oil of the SMEMG was lost and then self-replenished, the formed *R*-SMEMG surface element composition was basically the same as the initial SMEMG surface element composition. Therefore, it is considered that the VO inside the bulk of substrate self-filled the material surface in response to the UV irradiation, forming

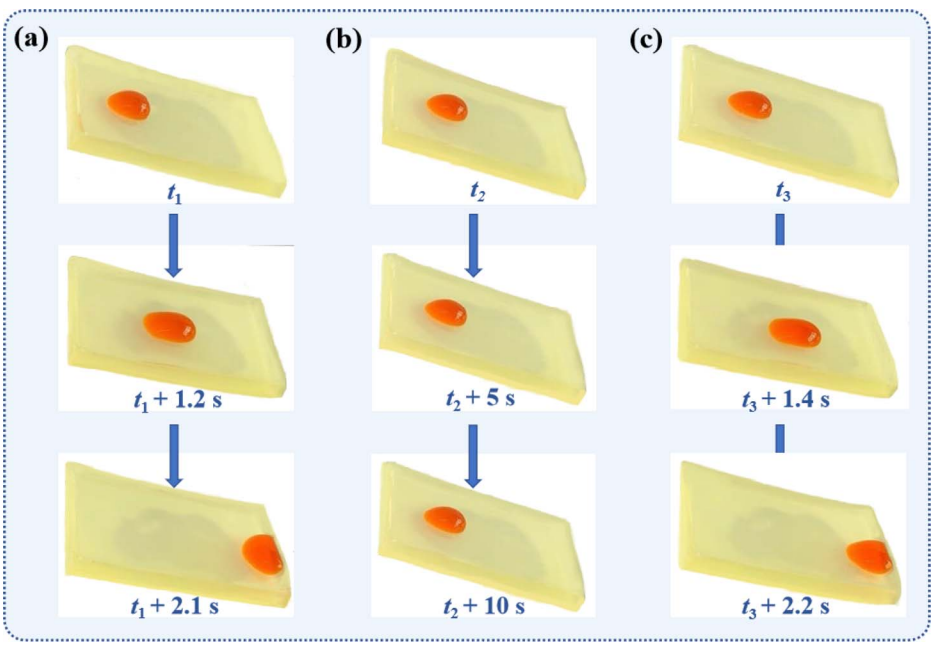


Fig. 7 Dynamic control of the mobility of a water droplet (20 μL) on the SMEMG. (a) Process of a water droplet slipping off the SMEMG at the initial state. (b) Process of a water droplet pinned on the SMEMG after the surface lubricant oil was swabbed. (c) Process of a water droplet re-sliding down the SMEMG after UV irradiation for 3 h.

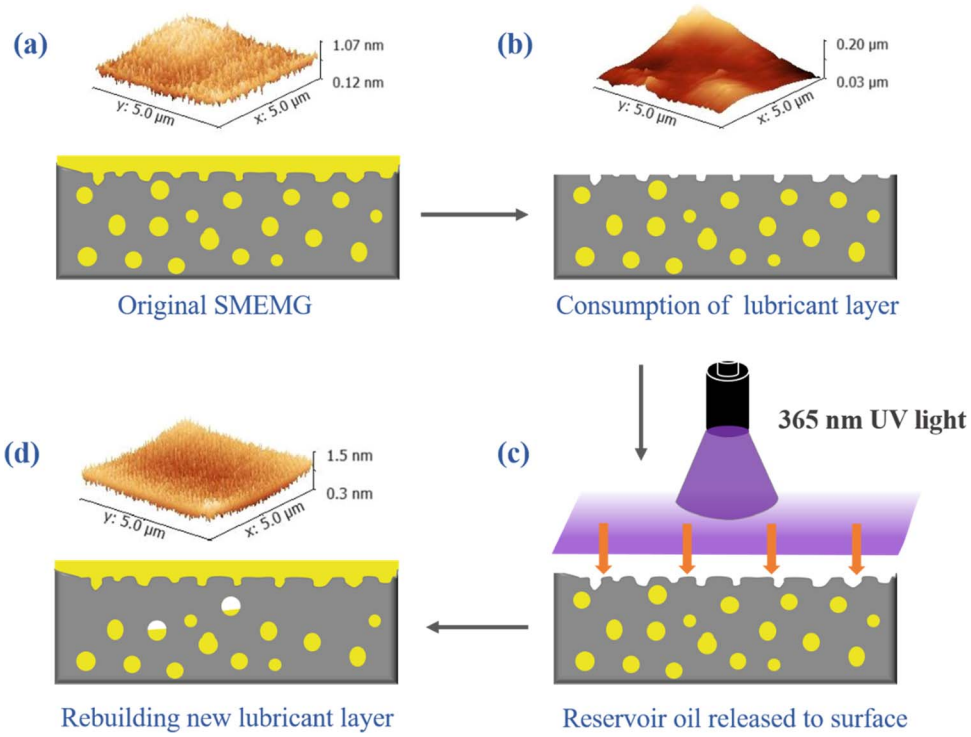


Fig. 8 Schematic of the consumption and rebuilding process of the lubricant layer on the surface of the SMEMG. (a) Distribution of the lubricant oil on the original SMEMG and the corresponding 3D AFM image, RMS: 0.12 nm; (b) consumption of the surface lubricant layer of the SMEMG and the corresponding 3D AFM image, RMS: 27.5 nm; (c) reservoir lubricant oil in the bulk of the substrate was released to the surface of the destroyed SMEMG under UV light irradiation at 365 nm wavelength; (d) rebuilding of a new lubricant layer on the destroyed SMEMG and the corresponding 3D AFM image, RMS: 0.16 nm.

a new lubricant layer. As shown in Fig. 8d, the roughness of the recovered SMEMG was decreased to 0.16 nm. Hence, the hysteresis angle of a sliding droplet would be highly declined, and then the water droplet could move along the surface.

The mechanism of the lubricant oil self-replenishing in this system is illustrated in Fig. 9. Under UV light irradiation at a wavelength of 365 nm, the adjacent coumarin groups in the side chain of the polymer would undergo photodimerization,

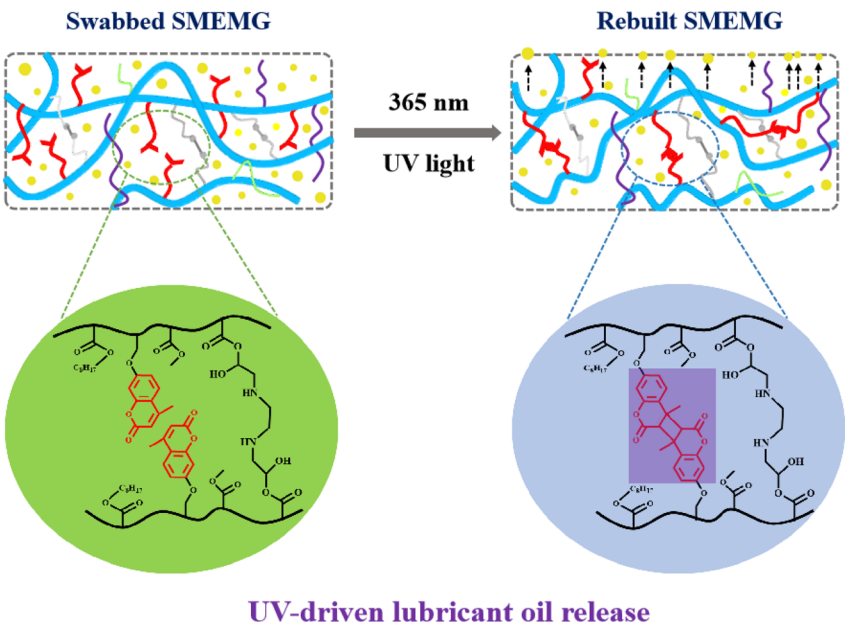


Fig. 9 Lubricant oil self-replenishing mechanism of the SMEMG.

thus enhancing the crosslinking degree of the network, and then advancing the extrusion of VO in the bulk of the SMEMG to the surface to construct a new lubricant layer, thereby promoting the recovery of the surface dewetting performance. Notably, the swabbed SMEMG was first treated under UV light at 254 nm for 30 min before 365 nm UV light treatment to facilitate the photodepolymerization of the coumarin groups. To further prove the influence of the coumarin groups on the self-replenishing performance of the SMEMG, the UV-responsive capacity of the SEMG was detected as the control test (Fig. S3†). As shown in the result, the original SEMG possessed good slippery performance. A water droplet could be removed

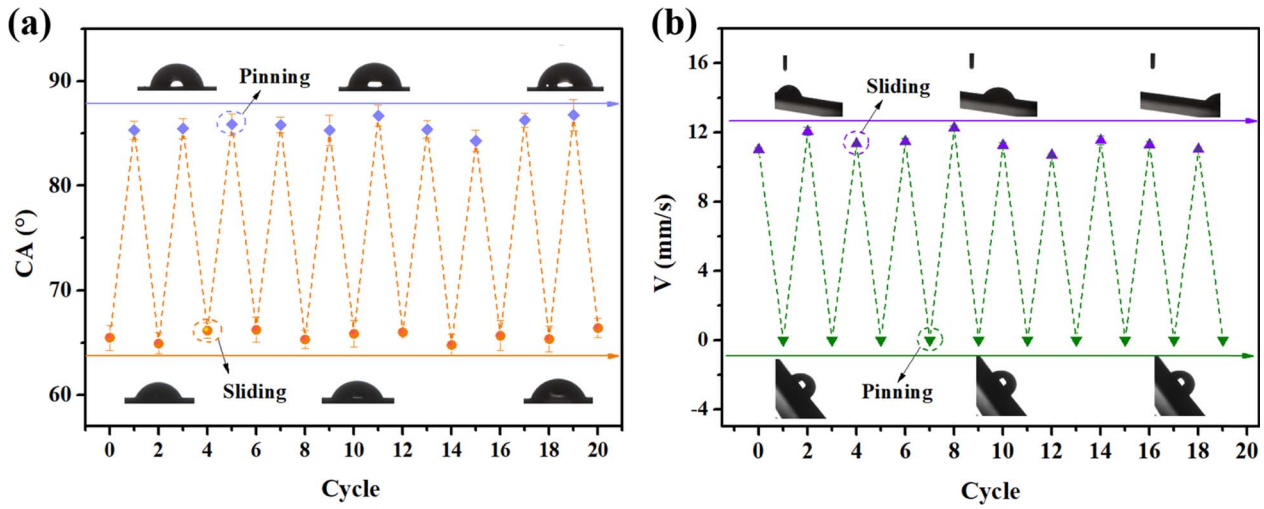


Fig. 10 CA (a) and sliding velocity (b) changes on the SMEMG as a function of repeated swabbing and UV light irradiation at 365 nm wavelength for 3 h; inset images in (a) show the CA images and in (b) the water droplet sliding motion on the SMEMG.

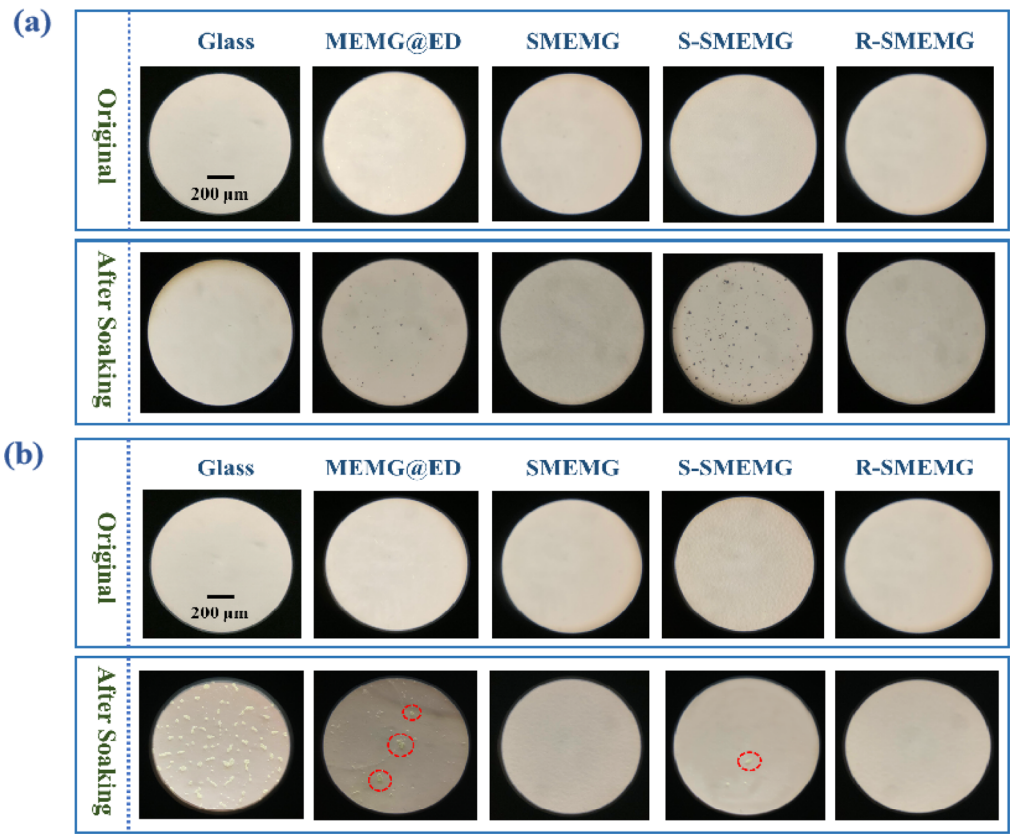


Fig. 11 Anti-algal tests of different samples. (a) Anti-diatom test; (b) anti-chlorella test. *S*-SMEMG refers to the SMEMG without a lubrication layer and *R*-SMEMG refers to the lubricant oil self-replenished slippery surface based on a damaged SMEMG.

away from the surface of the SEMG within 2.2 s, leaving no trace. Then, the droplet pinned on the surface when the liquid layer of the SEMG was lost. However, the water droplet remained pinned on the surface of the SEMG after the damaged SEMG was illuminated under UV light for 8 h. Emphatically, the fabrication of the SEMG was the same as that of the SMEMG but without the introduction of MHML. In addition, no obvious absorption peak was observed in the fluorescence spectra of EMG (Fig. S2d†), verifying that the SEMG without MHML was unable to respond to the UV light irradiation. Therefore, it seems that the coumarin groups on MHML endowed the SMEMG with a superb UV-responsive capacity. Hereafter, serial swabbing-UV illumination tests were performed to evaluate the lubricant oil-releasing durability. As shown in Fig. 10, during the 10 cycles of the swabbing and releasing process, the CA and water sliding velocity of the SMEMG just showed a slight fluctuation. After 10 cycles, the CA of the SMEMG was maintained at 66.41° and the water droplet sliding velocity remained at 11.02 mm $s^{-1}$, suggesting the VO could be repeatedly replenished to the surface and then the dewetting performance of the SMEMG could be recovered. The excellent durability of the lubricant oil-releasing capability benefited from the good compatibility between the VO and MEMG@ED and will highly advance the actual application of SLIPS materials.

### 3.5 Anti-algal adhesion performance

In this work, the anti-algal adhesion performance of the SMEMG surface was investigated using diatom and chlorella as biological fouling models. As shown in Fig. 11a, after soaking in diatom solution for 24 h and simple washing, there was almost no diatoms attached on the surface of the glass sheet, while a certain amount of diatoms were observed on the MEMG@ED surface. This could be attributed to the hard shells of the diatoms, which tend to adhere to softer material surfaces. Meanwhile, a large number of chlorella was found adhered to the surface of the glass sheet (Fig. 11b), probably because chlorella is soft and easy to deform, making it easier to adhere to the hard surface. In addition, no attached diatoms or chlorella were found on the surface of the SMEMG. Due to the excellent stability of the SMEMG, the lubricating layer remained securely anchored on the substrate surface in flowing water. The smooth surface structures and flowing water prevented algae from adhering. However, prolonged soaking eventually led to a loss of the surface lubrication layer on the SMEMG, resulting in significant algae attachment on the lubrication-lacking surface (S-SMEGMA). Nevertheless, due to its self-replenishing capability with lubricant oil, under UV light exposure, SMEMG released the internal lubricant onto its surface forming a new lubrication layer that restored its anti-algal adhesion performance; thus, preventing adherence to newly formed *R*-SMEMG surfaces.

## 4 Conclusions

In this paper, a UV-responsive slippery surface (SMEMG) was constructed by introducing the coumarin group into the side chain of a polymer. Both polymer substrates MEMG@ED and the slippery surface SMEMG exhibited excellent self-healing properties. Upon exposure of UV light, the broken MEMG@ED and SMEMG could be completely repaired while maintaining their mechanical and slippery properties. The intelligent control of a droplet movement on the SMEMG could be realized by controlling the release of lubricant under UV irradiation due to its exceptional lubricant self-replenishing properties. Furthermore, the outstanding anti-algal adhesion performance demonstrated that the SMEMG has potential in the field of marine anti-fouling.

## Data availability

The authors confirm that the data supporting the findings of this study are available within the article and the ESI.†

## Conflicts of interest

There are no conflicts to declare.

## Acknowledgements

This work was supported by the State Grid Corporation of China Headquarters Science and Technology Project [5108-202218280A-2-326-XG].

## References

1 J. Dong and J. Zhang, *Sci. Rep.*, 2018, **8**, 12062.
2 X. Li, Y. Li, I. Muzammil and M. Lei, *Plasma Processes Polym.*, 2020, **17**, 2000050.
3 D. Wang, Q. Sun, M. J. Hokkanen, C. Zhang, F.-Y. Lin, Q. Liu, S.-P. Zhu, T. Zhou, Q. Chang, B. He, Q. Zhou, L. Chen, Z. Wang, R. H. A. Ras and X. Deng, *Nature*, 2020, **582**, 55–59.
4 H. An, N. Jia, S. Wang, Z. Peng and S. Chen, *Bioinspiration Biomimetics*, 2022, **17**, 066005.
5 C. Yu, S. Sasic, K. Liu, S. Salameh, R. H. A. Ras and J. R. van Ommen, *Chem. Eng. Res. Des.*, 2020, **155**, 48–65.
6 Q. Wu, H. Yan, L. Chen, S. Qi, T. Zhao, L. Jiang and M. Liu, *Adv. Mater.*, 2023, **35**, 2212246.
7 H. Du, F. Liu and H. Wang, *J. Colloid Interface Sci.*, 2022, **616**, 720–729.
8 H. F. Bohn and W. Federle, *Proc. Natl. Acad. Sci. U.S.A.*, 2004, **101**, 14138–14143.
9 T.-S. Wong, S. H. Kang, S. K. Y. Tang, E. J. Smythe, B. D. Hatton, A. Grinthal and J. Aizenberg, *Nature*, 2011, **477**, 443–447.
10 X. Zeng, Z. Guo and W. Liu, *Bio-Des. Manuf.*, 2021, **4**, 506–525.
11 U. Manna, N. Raman, M. Welsh, Y. Zayas, H. Blackwell, S. Palecek and D. Lynn, *Adv. Funct. Mater.*, 2016, **26**, 3599–3611.
12 S. Amini, S. Kolle, L. Petrone, O. Ahanotu, S. Sunny, C. N. Sutanto, S. Hoon, L. Cohen, J. C. Weaver, J. Aizenberg, N. Vogel and A. Miserez, *Science*, 2017, **357**, 668–673.

13 S. Basu, B. M. Hanh, J. Q. Isaiah Chua, D. Daniel, M. H. Ismail, M. Marchioro, S. Amini, S. A. Rice and A. Miserez, *J. Colloid Interface Sci.*, 2020, **568**, 185–197.
14 Y. Yu, B. Jin, M. I. Jamil, D. Cheng, Q. Zhang, X. Zhan and F. Chen, *ACS Appl. Mater. Interfaces*, 2019, **11**, 12838–12845.
15 W. S. Y. Wong, K. I. Hegner, V. Donadei, L. Hauer, A. Naga and D. Vollmer, *Nano Lett.*, 2020, **20**, 8508–8515.
16 W. Cui and T. A. Pakkanen, *J. Colloid Interface Sci.*, 2020, **558**, 251–258.
17 S. Sunny, N. Vogel, C. Howell, T. L. Vu and J. Aizenberg, *Adv. Funct. Mater.*, 2014, **24**, 6658–6667.
18 J. Li, E. Ueda, D. Paulssen and P. A. Levkin, *Adv. Funct. Mater.*, 2019, **29**, 1802317.
19 J. Wang, W. Gao, H. Zhang, M. Zou, Y. Chen and Y. J. S. A. Zhao, *Sci. Adv.*, 2018, **4**, eaat7392.
20 X. Wang, Z. Wang, L. Heng and L. Jiang, *Adv. Funct. Mater.*, 2020, **30**, 1902686.
21 D. P. Regan and C. Howell, *Curr. Opin. Colloid Interface Sci.*, 2019, **39**, 137–147.
22 B. Shang, M. Chen and L. Wu, *ACS Appl. Mater. Interfaces*, 2018, **10**(37), 31777–31783.
23 J. Li, H. Zhao and L. Wang, *Adv. Mater. Interfaces*, 2021, **8**, 2100561.
24 Z. Li, W. Wu, J. Sun, J. Li and D. Zhang, *Chem. Eng. J.*, 2023, **470**, 144173.
25 L. Sun, Y. Wang, X. Zhang, F. Bian, L. Shang, Y. Zhao and W. Sun, *Chem. Eng. J.*, 2021, **426**, 131641.
26 X. Zhu, J. Lu, X. Li, B. Wang, Y. Song, X. Miao, Z. Wang and G. Ren, *Ind. Eng. Chem. Res.*, 2019, **58**, 8148–8153.
27 L. Zhou, H. Liu, A. Liu, L. Zhou, C. Du and Y. Li, *Appl. Surf. Sci.*, 2022, **579**, 152069.
28 S. Misra, M. Tenjimbayashi, W. Weng, S. Mitra and M. Naito, *ACS Appl. Mater. Interfaces*, 2023, **15**, 36839–36855.
29 G. Liu, J. Yang, K. Zhang, H. Yan, Y. Yan, Y. Zheng, L. Zhang, Z. Zhao, L. Wang, G. Yang and H. Chen, *Chem. Eng. J.*, 2024, **483**, 149192.
30 X. Zhou, P. Sudersan, D. Diaz, B. Leibauer, C. Hinduja, F. Darvish, P. Bista, L. Hauer, M. Wagner, W. Steffen, J. Liu, M. Kappl and H.-J. Butt, *Droplet*, 2024, **3**, e103.
31 J. Yu, R. Zhao, J. Wang, N. Wang, J. Xu, M. Jin and Y. Zhao, *Tribol. Int.*, 2024, **192**, 109220.
32 J. Liu, L. Ye, Y. Sun, M. Hu, F. Chen, S. Wegner, V. Mailänder, W. Steffen, M. Kappl and H.-J. Butt, *Adv. Mater.*, 2020, **32**, 1908008.
33 Z. Chen, H.-Y. Xie, Y.-J. Li, G.-E. Chen, S.-J. Xu and Z.-L. Xu, *J. Membr. Sci.*, 2021, **638**, 119704.
34 T. Zhang, Q. Liu, F. Meng, Y. Hou, M. K. H. Leung, Y. Wen and Q. Zhang, *Prog. Org. Coat.*, 2024, **186**, 107923.
35 Q. Rao, J. Zhang, X. Zhan, F. Chen and Q. Zhang, *J. Mater. Chem. A*, 2020, **8**, 2481–2489.
36 R. Deng, T. Shen, H. Chen, J. Lu, H.-C. Yang and W. Li, *J. Mater. Chem. A*, 2020, **8**, 7536–7547.
37 J. Ling, M. Z. Rong and M. Q. Zhang, *Polymer*, 2012, **53**, 2691–2698.
38 K. Yabuuchi, N. Matsuo, H. Maeda and M. Moriyama, *Polym. J.*, 2018, **50**, 1093–1097.
39 Y. Zhao, D. Vuluga, L. Lecamp and F. Burel, *RSC Adv.*, 2016, **6**, 32098–32105.